ACS APPLIED MATERIALS & INTERFACES

Letter

Cite This: ACS Appl. Mater. Interfaces 2018, 10, 12311−12316

www.acsami.org

Lipid-Modified Graphene-Transistor Biosensor for Monitoring Amyloid-β Aggregation

Chia-Jung Kuo,[†,‡] Hsu-Cheng Chiang,[†,‡] Chi-Ang Tseng,[‡] Chin-Fu Chang,[‡] Rajesh Kumar Ulaganathan,[‡] Tzu-Ting Ling,[‡] Yu-Jen Chang,[§] Chiao-Chen Chen,[‡] Yun-Ru Chen,[§] and Yit-Tsong Chen*[,‡,⊥]

[‡]Department of Chemistry, National Taiwan University, No. 1, Sec. 4, Roosevelt Road, Taipei 106, Taiwan

[§]Genomics Research Center, Academia Sinica, No. 128, Academia Road, Sec. 2, Nankang, Taipei 115, Taiwan

[⊥]Institute of Atomic and Molecular Sciences, Academia Sinica, P.O. Box 23-166, Taipei 106, Taiwan

Supporting Information

ABSTRACT: A graphene field-effect transistor (G-FET) with the spacious planar graphene surface can provide a large-area interface with cell membranes to serve as a platform for the study of cell membrane-related protein interactions. In this study, a G-FET device paved with a supported lipid bilayer (referred to as SLB/G-FET) was first used to monitor the catalytic hydrolysis of the SLB by phospholipase D. With excellent detection sensitivity, this G-FET was also modified with a ganglioside G_{M1}-enriched SLB (G_{M1}-SLB/G-FET) to detect cholera toxin B. Finally, the GM1-SLB/G-FET was employed to monitor amyloid-beta 40 (Aβ40) aggregation. In the early nucleation stage of Aβ40 aggregation, while no fluorescence was detectable with traditional thioflavin T (ThT) assay, the prominent electrical signals probed by G_{M1}-SLB/G-FET demonstrate that the G-FET detection is more sensitive than the ThT assay. The comprehensive kinetic information during the Aβ40 aggregation could be collected with a G_{M1}-SLB/G-FET, especially covering the kinetics involved in the early stage of Aβ40 aggregation. These experimental results suggest that SLB/G-FETs hold great potential as a powerful biomimetic sensor for versatile investigations of membrane-related protein functions and interaction kinetics.

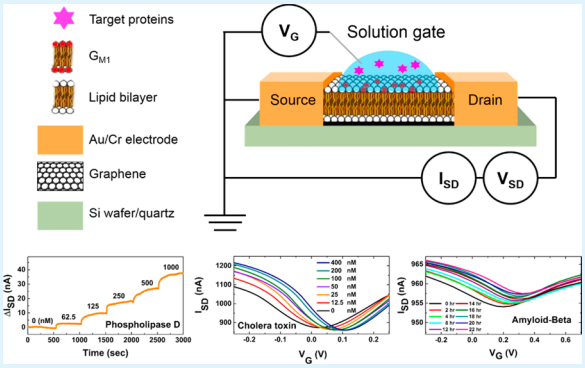

KEYWORDS: *graphene, field-effect transistor, biosensor, ganglioside GM1, supported lipid bilayer, phospholipase D, cholera toxin, amyloid-beta*

Graphene is a two-dimensional (2D) single-atom-thick carbon material, on which every atom is exposed on its surface. This 2D crystal possesses extremely high charge-carrier mobility, chemical robustness, high transmittance, and large specific surface area.[1] When graphene nanosheets are used as a conducting channel to fabricate a field-effect transistor (referred to as G-FET), this G-FET is highly sensitive and can detect environmental changes on the device's surface and serve as a biosensor for low noise and ultrasensitive detection.[2] In recent biological employments, G-FETs were demonstrated to be a successful biosensing platform for biomolecular recognition and cellular investigations, such as DNA−DNA hybridization,[3] PNA−DNA hybridization,[4] bacterial metabolic activities,[5] and aptamer−protein interactions.[6]

Benefiting from its spacious planar surface, a G-FET can provide a large-area interface with cell membranes and is suitable for the study of cell membrane-related protein interactions. For example, a G-FET device could be paved with a supported lipid bilayer (SLB) that contains receptor molecules of interest (referred to as SLB/G-FET) to offer several sensory advantages. First, the direct deposition of SLB on a G-FET provides a noncovalent modification on the graphene surface, thus retaining the excellent intrinsic electronic properties of the G-FET, e.g., high charge-carrier mobility, detection sensitivity, etc. Second, lipid bilayers are the primary composition of a cell membrane, which is involved in a variety of active biological events, such as biomolecular recognition, ion conductivity, and cell signaling. Therefore, developing a suitable SLB-containing biosensor is highly desirable for studying membrane protein interactions. Third, an artificial cell membrane of SLB that can maintain both integral membrane proteins and their functions is suitable for biological applications.[7] Moreover, the SLBs, situated on a planar solid support, could further increase their membrane stability. Compared with one-dimensional nanowire-/nanotube-based FET biosensors, 2D G-FETs possess a large, continuous interfacing area, thus offering a superior integration with lipid bilayers for membrane-related studies.[8,9] In addition,

Received: February 2, 2018
Accepted: April 3, 2018
Published: April 3, 2018

DOI: 10.1021/acsami.8b01917
ACS Appl. Mater. Interfaces 2018, 10, 12311−12316

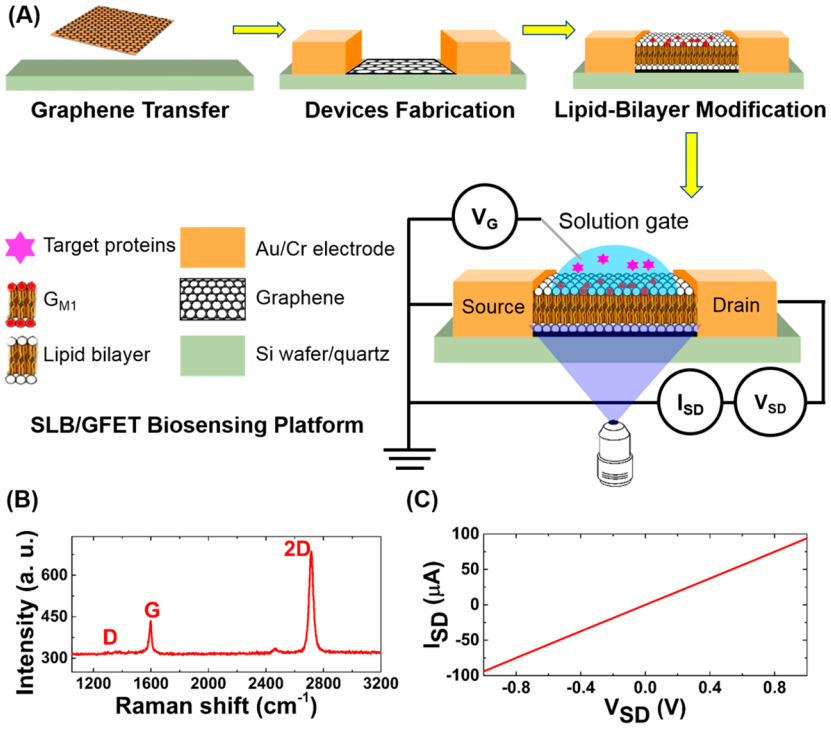

Figure 1. (A) Schematic illustration of preparing an SLB/G-FET device with a solution-gate electrode. The SLB/G-FET can be used as a biomimetic platform to detect the hydrolysis of SLB by a catalytic PLD. Moreover, ganglioside G_{M1} can be embedded in the SLB/G-FET to form a G_{M1}-SLB/G-FET for detecting CTxB or Aβ40 aggregation. The high spectral transmittance of graphene also makes the simultaneous detections of both fluorescence and electrical signals possible. (B) Intensity ratio of $I_{2D}/I_G \approx 3.6$ and the absence of the D band were observed in the Raman spectrum of CVD-grown graphene. (C) Linear $I_{SD}-V_{SD}$ plot measured in a G-FET device indicates an excellent ohmic-contact of the device.

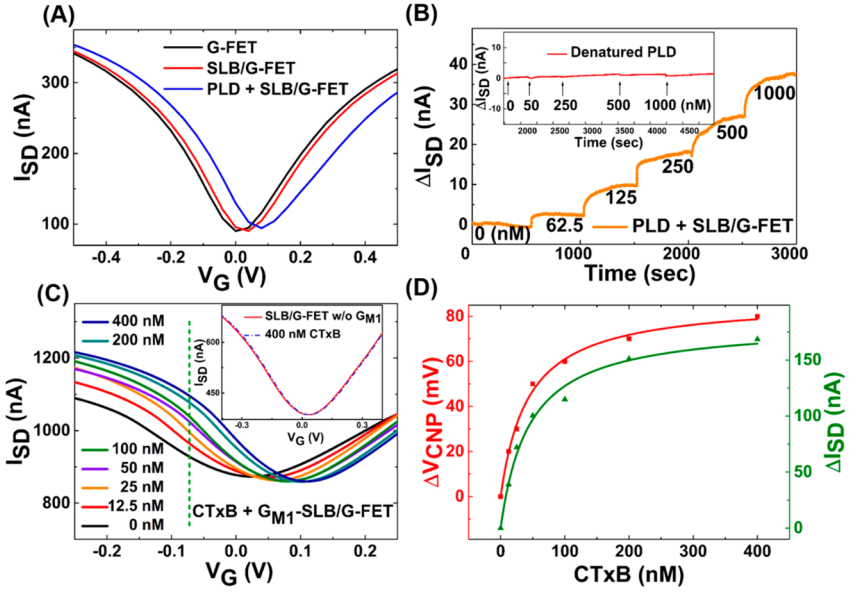

Figure 2. (A) Transfer curves of a bare G-FET (black curve) and an SLB/G-FET (red curve), where a slight p-doping of the G-FET by SLB caused a positive shift of the CNP by ~15 mV. After adding 1 μM of PLD to the SLB/G-FET (blue curve), a further positive shift of the CNP by ~55 mV was induced by the negatively charged PA, resulting from the hydrolysis of SLB by PLD (Figure S6). (B) Real-time current change of an SLB/G-FET (measured at V_G = 0 V) was measured in response to various C_{PLD} (62.5 nM−1 μM). In the inset, a control experiment of adding thermally denatured PLD to an SLB/G-FET demonstrates that no significant current change was observed. (C) Transfer curves of a G_{M1}-SLB/G-FET were recorded after each addition of CTxB (up to 400 nM) for 15 min incubation. In the inset, a control experiment of using an SLB/G-FET without modifying G_{M1} to detect CTxB shows no change in the transfer curve. (D) $\Delta V_{CNP}-C_{CTxB}$ (red squares) and $\Delta I_{SD}-C_{CTxB}$ (green triangles) plots represent, respectively, the CNP shift and current change as a function of C_{CTxB} measured in C. The ΔI_{SD} values at V_G = −0.07 V (marked by a vertical dashed green line in C) were chosen because the transfer curves are close to their linear regions. The Hill-Waud binding model was used to fit the $\Delta V_{CNP}-C_{CTxB}$ and $\Delta I_{SD}-C_{CTxB}$ experimental data, yielding the dissociation constants (K_d) of the CTxB-G_{M1} complex to be 52.2 ± 7.2 nM and 43.0 ± 3.7 nM, respectively.

DOI: 10.1021/acsami.8b01917
ACS Appl. Mater. Interfaces 2018, 10, 12311−12316

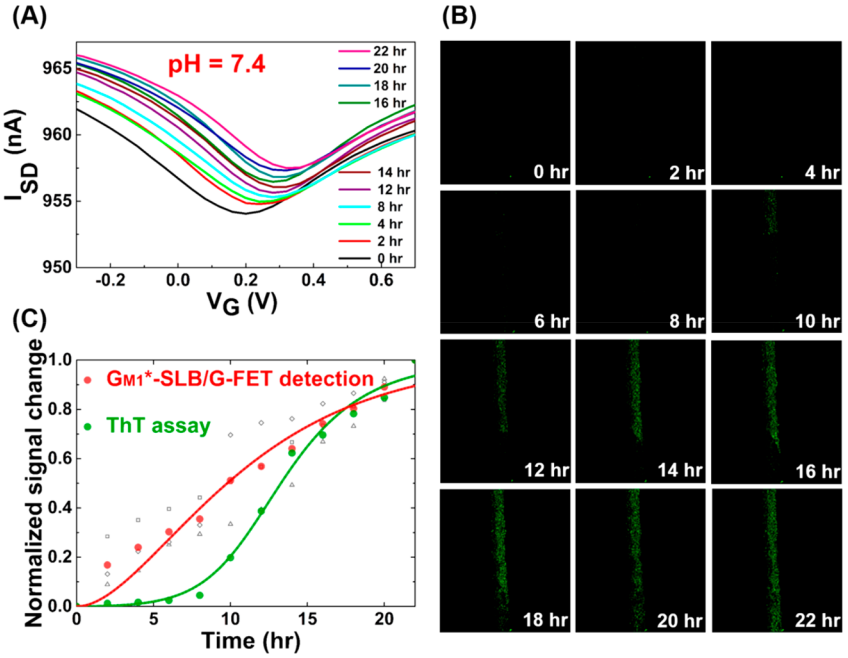

Figure 3. Simultaneous detections of the Aβ40 aggregation by both G_{M1}*-SLB/G-FET and ThT assay. (A) Changes of the transfer curve of a G_{M1}*-SLB/G-FET were recorded for 22 h by introducing 12.5 μM of Aβ40 solution at pH 7.4. The gradual aggregation of the negatively charged Aβ40 (pI = 5.3) induced a p-doping to the G_{M1}*-SLB/G-FET. (B) ThT assay on the same G_{M1}*-SLB/G-FET device recorded at 1.5 s/frame, where the fluorescence images were obtained by collecting 450−550 nm emission from the ThT dye excited at 405 nm. (C) Comparison of the observed signals by ThT assay (green dots) and G_{M1}*-SLB/G-FET (red dots) during the Aβ40 aggregation. Whereas the data points of the ThT assay (green dots) were collected from each frame in B by integrating the fluorescence intensity, those of G_{M1}*-SLB/G-FET (red dots) were an average of three measurements (represented by gray hollow squares, triangles, and diamonds). A kinetic model[30] was used to analyze the experimental data, where the red curve (G_{M1}*-SLB/G-FET) and green curve (ThT assay) represent the results of a least-squares fit to the model.

the high spectral transmittance of graphene also makes the fluorescence imaging on an SLB/G-FET attainable, providing the advantages of detecting both fluorescence and electrical signals simultaneously in the same SLB/G-FET device (Figure 1A), as will be demonstrated later.

To date, several works of using SLB/G-FETs for biological studies have been reported. Ang et al. investigated the transfer characteristics of an SLB/G-FET and used the SLB/G-FET to examine the activities of antimicrobial peptides.[10] Wang et al. introduced pore-forming membrane proteins on an SLB/G-FET to measure ion channel currents.[11] Despite these exciting studies, SLB/G-FETs have not been employed as affinity-based biosensors for membrane-related biomolecular recognitions. In this study, we took advantage of the label-free, sensitive, and real-time biosensing detections of SLB/G-FETs to investigate membrane protein interactions. Moreover, SLB/G-FETs can also integrate with other cell membrane molecules, such as glycolipids, carbohydrates, and cholesterol, to provide diverse biological functions for studying protein−protein interactions. To this end, we employed an SLB/G-FET to test its detection sensitivity by monitoring the catalytic hydrolysis of the SLB by phospholipase D (PLD). We also enriched an SLB with ganglioside G_{M1} to form a G_{M1}-SLB/G-FET for detecting cholera toxin B (CTxB) and monitoring the amyloid-beta 40 (Aβ40) aggregation.

A schematic representation of the device fabrication of an SLB/G-FET and the experimental setup of utilizing an SLB/G-FET biosensor to study membrane protein interactions are illustrated in Figure 1A and described in Section S1 of the Supporting Information. In Figure 1B, the Raman spectrum of a graphene film synthesized with a chemical vapor deposition (CVD) method[12] was investigated, where the absence of the D band (at ∼1335 cm^{-1}) reveals the excellent crystallinity of the CVD-grown graphene and the peak intensity ratio of $I_{2D}/I_G \approx 3.6$ for the G band (at ∼1568 cm^{-1}) and 2D band (at ∼2677 cm^{-1}) indicates a monolayer structure.[13] For the electric characteristics of the as-fabricated G-FET device, the measured linear output curve (i.e., the source-drain current (I_{SD}) vs bias voltage (V_{SD}) plot, Figure 1C) exhibits an excellent ohmic-contact. Furthermore, in Section S2 of the Supporting Information, the preparation of an SLB/G-FET by depositing SLB on a G-FET with a vesicle fusion method,[14] the examination of the SLB thickness by atomic force microscopy (AFM), and the tests of the surface mobility and lateral fluidity of the SLB on the as-prepared SLB/G-FET with a fluorescence recovery after photobleaching (FRAP) method[15] are described.

To examine the detection sensitivity of an SLB/G-FET biosensor, we employed PLD to cleave the charged head groups of SLBs and monitored the charged state remained on the SLB/G-FET in real time. PLD can cleave the charged headgroup from a phospholipid (i.e., induce the hydrolysis of phosphatidylcholine (PC)) into a negatively charged phosphatidic acid (PA) and a positively charged choline (as depicted in Figure S6 of the Supporting Information). Shown in Figure 2A are the transfer curves (i.e., the source-drain current (I_{SD}) vs gate voltage (V_G) plots) of a bare G-FET (black curve) and an SLB/G-FET (red curve), where the positive shift of the charge neutrality point (CNP, i.e., the Dirac point) by ∼15 mV reflects a slight p-doping of SLB on G-FET.[16] After treating the SLB/G-FET with 1 μM of PLD for 40 min (blue curve in Figure 2A), the CNP further shift by ∼55 mV due to a gating effect of the negatively charged PA left in the SLB. The CNP values of a

DOI: 10.1021/acsami.8b01917
ACS Appl. Mater. Interfaces 2018, 10, 12311−12316

G-FET measured in this study were determined by fitting the experimental data to a formula as described in Section S4 of the Supporting Information. Figure 2B further shows the real-time monitoring of the catalytic reaction of an SLB/G-FET as a function of the PLD concentration (C_{PLD} = 62.5 nM−1 μM); for comparison, a control experiment was also performed by adding thermally denatured PLD (up to 1 μM) to an SLB/G-FET (the inset of Figure 2B). As a result, the negligible current changes of SLB/G-FET (<1.5 nA) by adding the denatured PLD are in sharp contrast to the prominent electrical responses with the same dose treatments of normal PLD. These results demonstrate the sensitive detecting capability of an SLB/G-FET biosensor.

The cholera toxin B subunit (CTxB), a toxin secreted from *Vibrio cholera*, binds specifically to the ganglioside G_{M1} on a cell membrane with a dissociation constant of ∼30 nM.[17] Therefore, the detection of CTxB by the G_{M1}-enriched SLB/G-FET (referred to as G_{M1}-SLB/G-FET) was adopted in this study to demonstrate the application of an SLB/G-FET for biological recognition in the protein interactions on a cell membrane. Figure 2C shows the transfer curves of a G_{M1}-SLB/G-FET as a function of the CTxB concentration (C_{CTxB} = 0−400 nM). Upon binding the G_{M1}-SLB/G-FET, the negatively charged CTxB (with an isoelectric point of pI ≈ 7) induced p-doping at the G-FET and resulted in positive shifts of the transfer curve. Meanwhile, a control experiment of an SLB/G-FET without modifying G_{M1} (presented in the inset of Figure 2C) shows no change of the transfer curve after adding 400 nM of CTxB, indicating the specific binding of CTxB to G_{M1}. Figure 2D summarizes the shifts of CNP (ΔV_{CNP}, red squares) and the changes of current (ΔI_{SD} at V_G = −0.07 V, green triangles) as a function of C_{CTxB} measured in Figure 2C. The dissociation constants of K_d = 43.0 ± 3.7 nM (from ΔV_{CNP}−C_{CTxB}, red line) and 52.2 ± 7.2 nM (from ΔI_{SD}−C_{CTxB}, green line) for the CTxB-G_{M1} complex were determined from the least-squares fits to the Hill-Waud binding model.[18] It is worth noting that a model fitting to the CNP shift (red line) or the current change (green line) yields a similar dissociation constant of the CTxB-G_{M1} complex, suggesting the fidelity of the electrical measurements by G_{M1}-SLB/G-FET.

The ganglioside G_{M1} also plays a role in the fibril formation of Aβ, which is considered to be a risk factor responsible for neurodegeneration and Alzheimer's disease.[19] Earlier studies show that Aβ peptides could aggregate on lipid microdomains containing ganglioside G_{M1}, sphingomyelin (SM), and cholesterol (Chol).[20−22] In the investigation of the fibril formation of Aβ, a thioflavin T (ThT) fluorescence assay has been widely used as "a gold standard" to stain and identify amyloid fibrils by observing the dramatic increase of the fluorescence intensity after ThT binds to the crossed beta-rich structure.[23] Although several mechanisms and models[24] have been put forward to analyze the fluorescence signals, the ThT assay failed to report the Aβ aggregation in the very early stage, which might lose the comprehensive picture of the Aβ oligomerization.[25,26] To observe the Aβ40 aggregation in this study, 1 mg/mL of liposome solution containing the concentration ratio of G_{M1}:SM:Chol = 4:3:3 was prepared to form a G_{M1}*-SLB/G-FET (where G_{M1}* represents the G_{M1}:SM:Chol ingredients to distinguish the aforementioned G_{M1}-SLB/G-FET). Figures S7−S8 present the characteristic features of a G_{M1}*-SLB/G-FET, including the FRAP measurement and AFM investigation, respectively. Figure 3A shows the transfer curves of a G_{M1}*-SLB/G-FET in response to the incubation of 12.5 μM of Aβ40 in a phosphate buffer solution. Because of the negatively charged Aβ40 (pI = 5.3), the Aβ40 aggregation gradually induced *p*-doping to the G_{M1}*-SLB/G-FET, resulting in a positive shift of the transfer curve. During the Aβ40 aggregation, the current of CNP (or the minimum conductivity of a G-FET) also changes because of the variations of impurity/residual charge density or chemical environment on the G-FET surface.[27−29] Two control experiments also demonstrate the specific binding of Aβ40 to G_{M1}*-SLB/G-FET, where neither a G_{M1}*-SLB/G-FET could detect a sample solution without Aβ40 (Figure S9A) nor an SLB/G-FET device without modifying G_{M1} could capture Aβ40 (Figure S9B). During the Aβ40 aggregation monitored by G_{M1}*-SLB/G-FET, a ThT fluorescence assay (Figure 3B) was also conducted simultaneously in the same device (as illustrated in Figure 1A). No significant fluorescence signals were detected in the early observation (<8 h in Figure 3B), which could be due to the fact that most Aβ40 in the early nucleation phase are in their monomer/oligomer form, resulting in no substantial ThT fluorescence because of lack of the crossed β-strand structure.[23]

Figure 3C compares the signals of Aβ40 aggregation detected by G_{M1}*-SLB/G-FET and ThT assay. In the early measurements (<8 h), while no significant fluorescence was detectable in the ThT assay (green dots), prominent electrical signals probed by G_{M1}*-SLB/G-FET (red dots) suggest that the G-FET detection is more sensitive than the ThT assay. For a further kinetic analysis, we attempted to fit both ThT assay and G-FET signals with a reported kinetic model,[30] containing the steps of nucleation, elongation, and secondary nucleation in the Aβ40 aggregation. The least-squares fits of experimental data to the kinetic model[30] are described in Section S6 of the Supporting Information. Briefly, the analysis reveals that the reaction orders of primary nucleation (n_c) were determined to be 2.1 ± 0.1 (by ThT assay) and 1.9 ± 0.1 (by G-FET), indicating a pair of monomers were involved to fold as a nucleus in the Aβ40 aggregation for the subsequent elongation. Second, the ratios of the rate constants (k_n/k_2) between the primary nucleation (k_n) of the early stage and the secondary nucleation (k_2) of the later Aβ40 aggregation were obtained to be 6.4 ± 0.9 × 10^{-10} (ThT assay) and 4.2 ± 0.5 × 10^{-8} (G-FET). A possible explanation for the much smaller k_n/k_2 value obtained by ThT assay is due to a lack of detectable fluorescence signals in the early stage of nucleation (k_n). In contrast, the G_{M1}*-SLB/G-FET could detect Aβ40 via the electric-field effect and any binding of monomers, oligomers, and (proto)fibrils on the surface of G_{M1}*-SLB/G-FET could cause the conductivity change inside the G-FET device. Consequently, the superior G-FET can be used to complement the ThT assay in detecting Aβ40 oligomers, especially in the early nucleation phase.

In summary, SLBs have been integrated with a G-FET to form an SLB/G-FET for detecting membrane protein interactions. The SLB/G-FET possessed excellent membrane stability and dynamic fluidity under a FRAP test. The electrical modulation of an SLB/G-FET by adding PLD to cleave the charged head groups of SLB demonstrated the SLB/G-FET a sensitive platform for biological applications. The specific detection of CTxB with a G_{M1}-SLB/G-FET allowed the determination of the dissociation constant of the CTxB-G_{M1} complex. The comprehensive kinetic information during the Aβ40 aggregation could be collected with a sensitive G_{M1}*-SLB/G-FET, especially covering the kinetics involved in the early stage of Aβ40 aggregation. These experimental results

DOI: 10.1021/acsami.8b01917
ACS Appl. Mater. Interfaces 2018, 10, 12311−12316

suggest that SLB/G-FETs can be used as a powerful biomimetic sensor for versatile investigations of membrane-related protein functions and interaction kinetics.

■ ASSOCIATED CONTENT

Supporting Information

The Supporting Information is available free of charge on the ACS Publications website at DOI: 10.1021/acsami.8b01917.

Figures S1−S10 and additional information (PDF)

■ AUTHOR INFORMATION

Corresponding Author

*E-mail: ytcchem@ntu.edu.tw.

ORCID

Chiao-Chen Chen: 0000-0002-7628-5706

Yun-Ru Chen: 0000-0002-6596-6338

Yit-Tsong Chen: 0000-0002-6204-8320

Author Contributions

†C.-J.K. and H.-C.C. contributed equally.

Notes

The authors declare no competing financial interest.

■ ACKNOWLEDGMENTS

This work was partially supported by the Ministry of Science and Technology of Taiwan under MOST 106-2627-M-002-035. We acknowledge technical support from the biophysical core facility at IAMS and the advanced nano/microfabrication and characterization lab at Academia Sinica.

■ REFERENCES

(1) Allen, M. J.; Tung, V. C.; Kaner, R. B. Honeycomb Carbon: A Review of Graphene. *Chem. Rev.* **2010**, *110*, 132−145.

(2) Ang, P. K.; Chen, W.; Wee, A. T. S.; Loh, K. P. Solution-Gated Epitaxial Graphene as pH Sensor. *J. Am. Chem. Soc.* **2008**, *130*, 14392−14393.

(3) Cai, B.; Wang, S.; Huang, L.; Ning, Y.; Zhang, Z.; Zhang, G. J. Ultrasensitive Label-Free Detection of PNA-DNA Hybridization by Reduced Graphene Oxide Field-Effect Transistor Biosensor. *ACS Nano* **2014**, *8*, 2632−2638.

(4) Dong, X.; Shi, Y.; Huang, W.; Chen, P.; Li, L. J. Electrical Detection of DNA Hybridization with Single-Base Specificity Using Transistors Based on CVD-Grown Graphene Sheets. *Adv. Mater.* **2010**, *22*, 1649−1653.

(5) Huang, Y.; Dong, X.; Liu, Y.; Li, L. J.; Chen, P. Graphene-Based Biosensors for Detection of Bacteria and Their Metabolic Activities. *J. Mater. Chem.* **2011**, *21*, 12358−12362.

(6) Ohno, Y.; Maehashi, K.; Matsumoto, K. Label-Free Biosensors Based On Aptamer-Modified Graphene Field-Effect Transistors. *J. Am. Chem. Soc.* **2010**, *132*, 18012−18013.

(7) Lundbaek, J. A.; Collingwood, S. A.; Ingolfsson, H. I.; Kapoor, R.; Andersen, O. S. Lipid Bilayer Regulation of Membrane Protein Function: Gramicidin Channels as Molecular Force Probes. *J. R. Soc., Interface* **2010**, *7*, 373−395.

(8) Roiter, Y.; Ornatska, M.; Rammohan, A. R.; Balakrishnan, J.; Heine, D. R.; Minko, S. Interaction of Nanoparticles with Lipid Membrane. *Nano Lett.* **2008**, *8*, 941−944.

(9) Nguyen, P.; Berry, V. Graphene Interfaced with Biological Cells: Opportunities and Challenges. *J. Phys. Chem. Lett.* **2012**, *3*, 1024−1029.

(10) Ang, P. K.; Jaiswal, M.; Lim, C. H. Y. X.; Wang, Y.; Sankaran, J.; Li, A.; Lim, C. T.; Wohland, T.; Barbaros, O.; Loh, K. P. A Bioelectronic Platform Using a Graphene− Lipid Bilayer Interface. *ACS Nano* **2010**, *4*, 7387−7394.

(11) Wang, Y. Y.; Pham, T. D.; Zand, K.; Li, J.; Burke, P. J. Charging the Quantum Capacitance of Graphene with a Single Biological Ion Channel. *ACS Nano* **2014**, *8*, 4228−4238.

(12) Chen, C. C.; Kuo, C. J.; Liao, C.-D.; Chang, C. F.; Tseng, C. A.; Liu, C. R.; Chen, Y. T. Growth of Large-Area Graphene Single Crystals in Confined Reaction Space with Diffusion-Driven Chemical Vapor Deposition. *Chem. Mater.* **2015**, *27*, 6249−6258.

(13) Graf, D.; Molitor, F.; Ensslin, K.; Stampfer, C.; Jungen, A.; Hierold, C.; Wirtz, L. Spatially Resolved Raman Spectroscopy of Single- and Few-Layer Graphene. *Nano Lett.* **2007**, *7*, 238−242.

(14) Tero, R.; Takizawa, M.; Li, Y. J.; Yamazaki, M.; Urisu, T. Lipid Membrane Formation by Vesicle Fusion on Silicon Dioxide Surfaces Modified with Alkyl Self-Assembled Monolayer Islands. *Langmuir* **2004**, *20*, 7526−7531.

(15) Braeckmans, K.; Peeters, L.; Sanders, N. N.; DeSmedt, S. C.; Demeester, J. Three-Dimensional Fluorescence Recovery after Photobleaching with the Confocal Scanning Laser Microscope. *Biophys. J.* **2003**, *85*, 2240−2252.

(16) Kiani, M.; Harun, F. K.; Ahmadi, M.; Rahmani, M.; Saeidmanesh, M.; Zare, M. Conductance Modulation of Charged Lipid Bilayer Using Electrolyte-Gated Graphene-Field Effect Transistor. *Nanoscale Res. Lett.* **2014**, *9*, 371.

(17) Williams, T. L.; Jenkins, A. T. A. Measurement of the Binding of Cholera Toxin to GM1 Gangliosides on Solid Supported Lipid Bilayer Vesicles and Inhibition by Europium (III) Chloride. *J. Am. Chem. Soc.* **2008**, *130*, 6438−6443.

(18) Moran-Mirabal, J. M.; Edel, J. B.; Meyer, G. D.; Throckmorton, D.; Singh, A. K.; Craighead, H. G. Micrometer-Sized Supported Lipid Bilayer Arrays for Bacterial Toxin Binding Studies through Total Internal Reflection Fluorescence Microscopy. *Biophys. J.* **2005**, *89*, 296−305.

(19) Mucke, L. Alzheimer's Disease. *Nature* **2009**, *461*, 895−897.

(20) Ikeda, K.; Yamaguchi, T.; Fukunaga, S.; Hoshino, M.; Matsuzaki, K. Mechanism of Amyloid β-Protein Aggregation Mediated by GM1 Ganglioside Clusters. *Biochemistry* **2011**, *50*, 6433−6440.

(21) Hoshino, T.; Mahmood, M. I.; Mori, K.; Matsuzaki, K. Binding and Aggregation Mechanism of Amyloid β-Peptides onto the GM1 Ganglioside-Containing Lipid Membrane. *J. Phys. Chem. B* **2013**, *117*, 8085−8094.

(22) Matsuzaki, K.; Noguch, T.; Wakabayashi, M.; Ikeda, K.; Okada, T.; Ohashi, Y.; Hoshino, M.; Naiki, H. Inhibitors of Amyloid β-Protein Aggregation Mediated by GM1-Containing Raft-Like Membranes. *Biochim. Biophys. Acta, Biomembr.* **2007**, *1768*, 122−130.

(23) Biancalana, M.; Koide, S. Molecular Mechanism of Thioflavin-T Binding to Amyloid Fibrils. *Biochim. Biophys. Acta, Proteins Proteomics* **2010**, *1804*, 1405−1412.

(24) Meisl, G.; Yang, X.; Frohm, B.; Knowles, T. P. J.; Linse, S. Quantitative Analysis of Intrinsic and Extrinsic Factors in the Aggregation Mechanism of Alzheimer-Associated Aβ-Peptide. *Sci. Rep.* **2016**, *6*, 18728.

(25) Garai, K.; Frieden, C. Quantitative Analysis of the Time Course of Aβ Oligomerization and Subsequent Growth Steps Using Tetramethylrhodamine-Labeled Aβ. *Proc. Natl. Acad. Sci. U. S. A.* **2013**, *110*, 3321−3326.

(26) Kumar, M.; Hong, Y.; Thorn, D. C.; Ecroyd, H.; Carver, J. A. Monitoring Early-Stage Protein Aggregation by an Aggregation-Induced Emission Fluorogen. *Anal. Chem.* **2017**, *89*, 9322−9329.

(27) Kim, B. H.; Hong, S. J.; Baek, S. J.; Jeong, H. Y.; Park, N.; Lee, M.; Lee, S. W.; Park, M.; Chu, S. W.; Shin, H. S.; Lim, J.; Lee, J. C.; Jun, Y.; Park, Y. W. N-Type Graphene Induced by Dissociative H2 Adsorption at Room Temperature. *Sci. Rep.* **2012**, *2*, 690.

(28) Tan, Y. W.; Zhang, Y.; Bolotin, K.; Zhao, Y.; Adam, S.; Hwang, E. H.; DasSarma, S.; Stormer, H. L.; Kim, P. Measurement of Scattering Rate and Minimum Conductivity in Graphene. *Phys. Rev. Lett.* **2007**, *99*, 246803.

(29) Adam, S.; Hwang, E. H.; Galitski, V.; Das Sarma, S. A Self-Consistent Theory for Graphene Transport. *Proc. Natl. Acad. Sci. U. S. A.* **2007**, *104*, 18392−18397.

DOI: 10.1021/acsami.8b01917
ACS Appl. Mater. Interfaces 2018, 10, 12311−12316

(30) Meisl, G.; Yang, X.; Hellstrand, E.; Frohm, B.; Kirkegaard, J. B.; Cohen, S. I. A.; Dobson, C. M.; Linse, S.; Knowles, T. P. J. Differences in Nucleation Behavior Underlie the Contrasting Aggregation Kinetics of the Aβ40 and Aβ42 Peptides. *Proc. Natl. Acad. Sci. U. S. A.* **2014**, *111*, 9384−9389.

DOI: 10.1021/acsami.8b01917
ACS Appl. Mater. Interfaces 2018, 10, 12311−12316